Journal of Magnetism and Magnetic Materials 587 (2023) 171322

Contents lists available at ScienceDirect

Journal of Magnetism and Magnetic Materials

journal homepage: www.elsevier.com/locate/jmmm

Research article

Strain-induced Aharonov-Bohm effect at nanoscale and ground state of a carbon nanotube with zigzag edges

Adam Rycerz *, Maciej Fidrysiak, Danuta Goc-Jagło

Institute for Theoretical Physics, Jagiellonian University, Łojasiewicza 11, PL–30348, Kraków, Poland

ARTICLE INFO

Keywords:
Graphene
Carbon nanotubes
Hubbard model
Mott transition
Aharonov–Bohm effect

ABSTRACT

Magnetic flux piercing a carbon nanotube induce periodic gap oscillations which represent the Aharonov-Bohm effect at nanoscale. Here we point out, by analyzing numerically the anisotropic Hubbard model on a honeycomb lattice, that similar oscillations should be observable when uniaxial strain is applied to a nanotube. In both cases, a vector potential (magnetic- or strain-induced) may affect the measurable quantities at zero field. The analysis, carried out within the Gutzwiller Approximation, shows that for small semiconducting nanotube with zigzag edges and realistic value of the Hubbard repulsion ($U/t_0 = 1.6$, with $t_0 \approx 2.5$ eV being the equilibrium hopping integral) energy gap can be reduced by a factor of more than 100 due to the strain.

1. Introduction

Aharonov-Bohm (AB) effect [1–3] represents one of the most spectacular features of quantum mechanics, as it demonstrate the physical meaningfulness of magnetic vector potential when the current flows entirely through zero magnetic field regions [4]. In the familiar *two-slit-like* setup, conducting region is pierced by magnetic flux and the quantum interference for an electron passing simultaneously the two distinct paths, encircling the flux, is observed. Since the discovery of graphene [5,6], several experimental and theoretical works have addressed specific features of AB effect in this two-dimensional form of carbon [7–16]. In particular, strain-induced pseudomagnetic potentials allow one to observe zero magnetic flux analogs of AB effects [15,16].

In its nanoscale version realized in carbon nanotubes [17–20], AB effect no longer requires a two-slit-like setup because the flux strongly affects electronic structure near the Fermi energy [17] (in principle, a semiconducting nanotube can be turned into the metallic one and *vice versa* [21]). This can be traced via measurable quantities for *closed* system rather than by detecting the quantum interference in an *open* system [20]. However, in typical measurements multiwalled nanotubes are used [18,19] and the mutual influence of dynamical and magnetic phase shifts [4] results in rather complex physics, showing some common features with quantum interference observed in metallic cylinders in Ref. [1].

Here, we discuss a nanoscale AB effect in a strained nanotube, following the analogy visualized in Fig. 1. The attention is focussed on zigzag nanotube, as the strain along armchair direction does not open an *intrinsic* (i.e., size-independent) gap in the single-particle spectrum [22] allowing also to complement the discussion on the role of electron correlations in graphene-related systems [23–26]. Our results show that strains earlier demonstrated for planar graphene samples [27,28], if accessed in a single-walled nanotube device, may result in significant, approximately periodic evolutions of the multiparticle ground state. For the Hubbard repulsion $U/t_0 = 1.6$ [24] (with $t_0 \approx 2.5$ eV the equilibrium hopping for nearest-neighbors) we predict the narrow Mott-insulating phase (MI), corresponding the strain adjusted such that a single-particle spectrum is gapless, to be surrounded with band-insulating phases (BI). A significant gap reduction in MI compared to BI allows to expect the former to behave almost as a semimetallic system in the presence of external bias voltage or thermal excitations.

The remaining part of the paper is organized as follows. In Section 2 we briefly present the effective Hubbard Hamiltonian and the Gutzwiller Approximation (GA). Also in Section 2, a simplified relation between the model parameters and geometric strains is put forward. In Section 3, we discuss our numerical results concerning the phase diagram of the effective Hubbard Hamiltonian adapted to model zigzag $(10, 0)$ nanotube subjected to the longitudinal strain, as well as the strain effect on multiparticle charge-energy gap. The conclusions are given in Section 4.

2. Model and methods

We write the Hamiltonian of the Hubbard model on anisotropic honeycomb lattice as $H = H_t + H_U$ [22,26], where the kinetic part

* Corresponding author.
E-mail address: rycerz@th.if.uj.edu.pl (A. Rycerz).

https://doi.org/10.1016/j.jmmm.2023.171322
Received 17 July 2023; Received in revised form 14 September 2023; Accepted 26 September 2023
Available online 28 September 2023

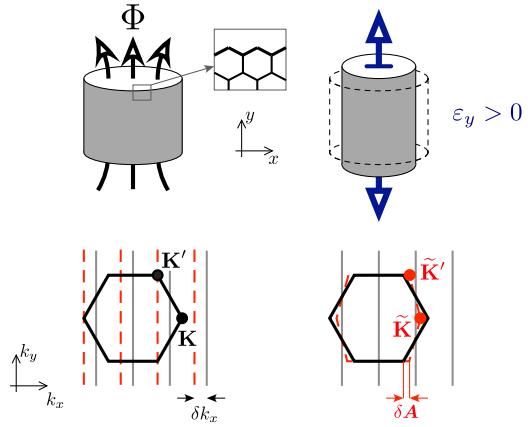

Fig. 1. Left: Magnetic flux Φ parallel to the main axis (y) of zigzag $(N_x, 0)$ nanotube (top) shifts the values of quantized transverse momenta, $k_x = 2\pi n_x/N_x$ with $n_x = 0, 1, \ldots, N_x - 1$, by $\delta k_x = 2\pi(e/h)\Phi/N_x$ (bottom). Right: In analogy, uniaxial strain $\varepsilon_y > 0$ affects the low-energy spectrum by shifting the Dirac points, $\boldsymbol{K}$ and $\boldsymbol{K}'$, by $\delta\boldsymbol{A} = (\mp\delta A_x, 0)$, with $\delta A_x \propto \varepsilon_y$ [see the main text for details]. Both mechanisms may lead to approximately periodic bandgap oscillations, with the minimum gap corresponding to a discrete value of k_x matching the Dirac point.

is

$$H_t = -t_x \sum_{\langle ij\rangle_x, s} (e^{i\phi} c^\dagger_{i,s} c_{j,s} + \text{H.c.}) - t_y \sum_{\langle ij\rangle_y, s} (c^\dagger_{i,s} c_{j,s} + \text{H.c.}) \tag{1}$$

and the interaction part is

$$H_U = U \sum_j n_{j\uparrow} n_{j\downarrow}. \tag{2}$$

Here, $c^\dagger_{i,s}$ ($c_{i,s}$) creates (annihilates) an electron at site i of the honeycomb lattice with spin $s = \uparrow$ or $\downarrow$, and $n_{is} = c^\dagger_{i,s} c_{i,s}$ is the particle number operator. t_x (t_y) is the nearest-neighbor hopping along (out of) the zigzag direction. The Peierls phase $\phi = \Phi/N_x$ with Φ being the magnetic flux parallel to y axis in a zigzag $(N_x, 0)$ geometry (see Fig. 1). In the interaction part, U is the on-site Hubbard repulsion and operator $n_{j\uparrow} n_{j\downarrow}$ measures the number of double occupancies. Throughout the paper, we focus on the ground-state phase diagram at half filling, for $\Phi = 0$ and $t_y \leqslant t_x$ (i.e., strain applied in the armchair direction).

Several approximate methods can be utilized to determine whether the ground state of the Hamiltonian H is conducting or insulating. Within the Gutzwiller Approximation (GA) [29,30] one needs to find the minimum of

$$\frac{E_G^{(\mathrm{GA})}}{N} = q(m,d) \times \left[-\frac{2}{N} \sum_{\mathbf{k}} \sqrt{E^2_{\mathbf{k}} + \left(\frac{Um}{2}\right)^2} + \frac{Um^2}{2} \right] + Ud, \tag{3}$$

with respect to the sublattice magnetization m (quantifying the antiferromagnetic order) and the average double occupancy d. The constrictions are $|m| \leqslant 1$ and $d \leqslant d_{\max} = \frac{1}{4}(1 - m^2)$. The band narrowing factor is given by

$$q(m,d) = \frac{4d}{1-m^2} \left[1 - 2d + \sqrt{(1-2d)^2 - m^2} \right]. \tag{4}$$

The summation in Eq. (3) runs over quasimomenta $\mathbf{k} \equiv (k_x, k_y)$ in the first Brillouin zone (see Fig. 2), namely

$$k_x = \frac{2\pi}{N_x}(n_x + \phi), \qquad k_y = \frac{4\pi}{\sqrt{3}} \left(\frac{n_y}{N_y} - \frac{n_x}{2N_x} \right), \tag{5}$$
$$n_x = 0, 1, \ldots, N_x - 1, \qquad n_y = 0, 1, \ldots, N_y - 1,$$

with $N_{x,y}$ being the number of unit cells in x, y direction, and $N = 2N_xN_y$ (the periodic boundary conditions are imposed). We further notice that setting $d = d_{\max}$ in Eqs. (3) and (4) reduces the procedure to the familiar Hartree–Fock approximation (HF) with the antiferromagnetic order at half filling, $\langle n_{i\uparrow}\rangle = \frac{1}{2}(1 \pm m)$ and $\langle n_{i\downarrow}\rangle = \frac{1}{2}(1 \mp m)$, where the upper (lower) sign corresponds to the sublattice A (B).

The single-particle energies for anisotropic honeycomb lattice are given by

$$E_{\mathbf{k}} = t_x \sqrt{a^2_{\mathbf{k}} + b^2_{\mathbf{k}}}, \tag{6}$$

with

$$a_{\mathbf{k}} = -\cos\left(\frac{k_x}{2} + \frac{\sqrt{3}k_y}{2}\right) - \cos\left(\frac{k_x}{2} - \frac{\sqrt{3}k_y}{2}\right) - \frac{t_y}{t_x},$$
$$b_{\mathbf{k}} = \sin\left(\frac{k_x}{2} + \frac{\sqrt{3}k_y}{2}\right) - \sin\left(\frac{k_x}{2} - \frac{\sqrt{3}k_y}{2}\right). \tag{7}$$

Also in Fig. 2, we display cross sections of $E_{\mathbf{k}}$ for $k_y = 0$ and $k_y = 2\pi/\sqrt{3}$ in the bulk limit (i.e., $N_x, N_y \to \infty$). In the vicinity of Dirac points, conical band structure gets shifted along the k_x axis by the value of strain-induced vector potential, for $|t_x - t_y| \ll t_x$,

$$\delta A_x \approx \mp \frac{2}{\sqrt{3}} \frac{t_x - t_y}{t_x} \approx \mp \frac{\sqrt{3}}{2} \beta \varepsilon_y (1 + \nu), \tag{8}$$

where the upper (lower) sign correspond to K (K') valley, $\beta \approx 2 - 3$ is the dimensionless electron–phonon coupling, ε_y is relative strain along the armchair direction, and $\nu = -\varepsilon_x/\varepsilon_y \approx 0.2 - 0.4$ is Poisson's ratio [31,32]. Deriving the second approximate equality in Eq. (8) we have parametrized the hopping elements according to [33,34]

$$t_{x,y} = -t_0 \left(1 - \beta \frac{\delta d_{x,y}}{d_0} \right), \tag{9}$$

where the relative bond elongations, i.e., $\delta d_{x,y} \equiv d_{x,y} - d_0$ with the equilibrium bond length d_0, can be written as

$$\frac{\delta d_x}{d_0} = \frac{1}{4}\varepsilon_y (1 - 3\nu) + \mathcal{O}(\varepsilon_y^2), \qquad \frac{\delta d_y}{d_0} = \varepsilon_y. \tag{10}$$

For a zigzag $(N_x, 0)$ geometry, k_x gets quantized according to Eq. (5) (hereinafter, we set $\phi = 0$) and k_y remains continuous due to $N_y \to \infty$. In turn, the appearance of gapless subbands is expected for

$$N_x \left(\frac{1}{3} + \frac{\delta A_x}{2\pi} \right) = m, \quad \text{with} \quad m \ \text{integer}. \tag{11}$$

In the absence of strain, $\delta A_x = 0$, the above reduces to $N_x = 3m$, restoring the standard condition for metallicity of carbon nanotubes with zigzag edges [35]. In Table 1, we go beyond the small-strain limit of Eq. (8), and present the values of t_y/t_x corresponding to vanishing single-particle gap,

$$\Delta E_{\mathrm{TBA}} \equiv 2 \min_{n_x, k_y} E_{\mathbf{k}} = 0, \tag{12}$$

which were obtained numerically for $10 \leqslant N_x \leqslant 20$. The case of $N_x = 10$, showing only one zero for $t_y/t_x = 0.618$ (corresponding to $\varepsilon_y \approx 0.15$), is chosen for further considerations.

3. Results and discussion

It is clear from Eq. (8) that dimensionless parameter $(t_x - t_y)/t_x \propto \varepsilon_y$ may be used to quantify uniaxial strain along the armchair direction. To quantify the Hubbard interaction, we choose U/t_x. (It can be shown that $t_x \approx t_0[1 - \frac{1}{4}\beta\varepsilon_y(1 - 3\nu)]$; therefore, for $\nu \approx 1/3$ the strain dependence is weak.)

Our central results are presented in Fig. 3, where we display the phase diagram for the Hamiltonian $H = H_t + H_U$, see Eqs. (1) and (2), and $N_x = 10$. The phases are identified by finding the optimal

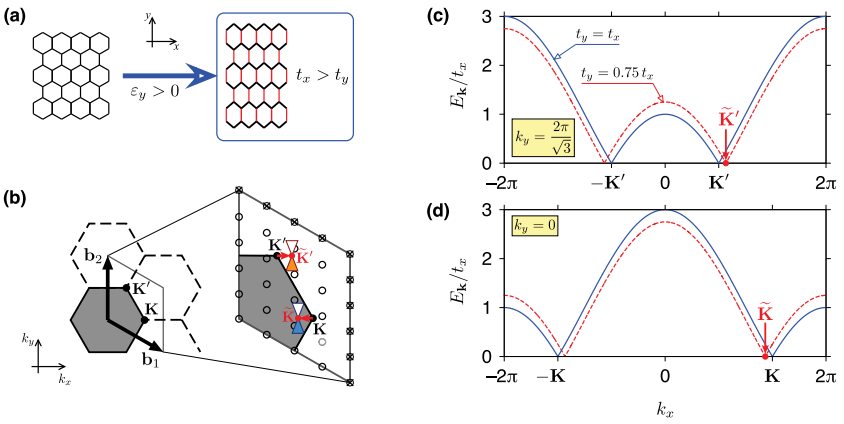

Fig. 2. (a) Honeycomb lattice subjected to uniaxial strain in the armchair direction. (b) Hexagonal first Brillouin zone (FBZ) of the reciprocal lattice, with (dimensionless) basis vectors $\mathbf{b}_1 = \left(2\pi/\sqrt{3}\right)(\sqrt{3}, -1)$ and $\mathbf{b}_2 = \left(2\pi/\sqrt{3}\right)(0, 2)$. The magnified area shows discretized FBZ for a finite system of $N = 2N_xN_y$ atoms with periodic boundary conditions [see Eq. (5)] with the Dirac points shifted the positions $\tilde{\boldsymbol{K}}$ and $\tilde{\boldsymbol{K}}'$ due to the strain. (c) Cross section of the bulk single-particle energy [see Eqs. (6) and (7)] for $k_y = 2\pi/\sqrt{3}$, matching the upper edge of FBZ. Blue solid line correspond to the lattice in equilibrium ($t_x = t_y$), red dashed is for the strain quantified by $t_y = 0.75\,t_x$. (d) Same as (c), but for $k_y = 0$.

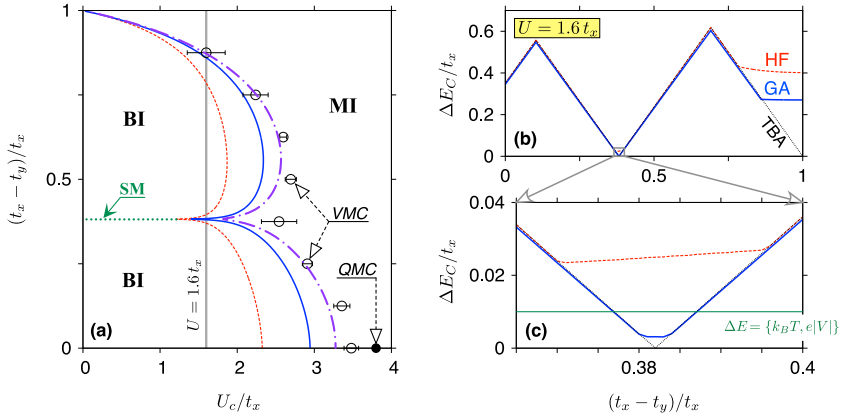

Fig. 3. (a) Phase diagram for the Hubbard model on anisotropic honeycomb lattice with $t_y \leqslant t_y$ [see Eqs. (1) and (2)] and the number of unit cell along the zigzag direction $N_x = 10$. Lines depict the critical Hubbard repulsion obtained within the Hartree–Fock method [red dashed], the Gutzwiller Approximation [blue solid], and Statistically-consistent GA [purple dash-dot]. Datapoints with errorbars are the results of VMC simulations for the Gutzwiller Wave Function reprinted from Ref. [26]. Quantum Monte Carlo value for the isotropic case ($t_x = t_y$), and the limit of $N_x, N_y \to \infty$ taken numerically, $U_c/t_0 = 3.86$ (see Ref. [23]), is marked with full circle. Remaining labels are: the band insulator (BI), the Mott insulator (MI), and the semimetal (SM) [mark with green dotted line corresponding to vanishing single-particle gap at $t_y/t_x = 0.618$, see Table 1]. Grey vertical line depicts the value of $U/t_x = 1.6$ used in remaining plots. (b) Charge gap as a function of strain for $U/t_x = 1.6$. Different lines correspond to the methods specified on the plot. (c) Zoom-in of (b) for the vicinity of $t_y/t_x = 0.618$. Green horizontal line at $\Delta E = 0.01\,t_x \approx 25\,\mathrm{meV}$ marks typical energy of quasiparticle excitations at $T = 300\,\mathrm{K}$. (We further notice that a comparable energy of $e|V|$ may also appear due to source–drain voltage difference.).

Table 1
Values of the hopping ratio corresponding to the vanishing single particle gap (ΔE_{TBA}) obtained from the anisotropic tight-binding Hamiltonian for small zigzag $(N_x, 0)$ nanotubes. Notice that metallic nanotubes ($N_x = 3$ m) show $\Delta E_{\mathrm{TBA}} = 0$ for $t_x = t_y$.

N_x	$(t_y/t_x)_{\Delta E_{\mathrm{TBA}}=0}$		
10	0.6180		
11	0.8308	0.2846	
12	1.0000	0.5176	
13	0.7092	0.2411	
14	0.8678	0.4450	
15	1.0000	0.6180	0.2091
16	0.7654	0.3902	
17	0.8915	0.5473	0.1845
18	1.0000	0.6840	0.3473
19	0.8034	0.4910	0.1652
20	0.9080	0.6180	0.3129

parameters (m, d) within GA. Blue solid line in panel (a) marks the border between the solutions with $m = 0$ and $m \neq 0$ (i.e, the critical value of $U_c^{(\mathrm{GA})}$). Similarly, by fixing the second parameter at $d = d_{\max}$ [see Eq. (3)], we determine the value of $U_c^{(\mathrm{HF})}$ (red dashed line). Purple dashed–dotted line marks the value of $U_c^{(\mathrm{SGA})}$ obtained within the *Statistically-consistent GA* [29], a method in which not only parameters (m, d) but also hopping integrals of the auxiliary Hamiltonian are optimized. It can be noticed that for $(t_x - t_y)/t_x \to 1$, all the methods leads to $U_c \to 0$, reproducing the value for decoupled Hubbard chains [36].

The solution with $m \neq 0$ is interpreted as the Mott insulator (MI). If $m = 0$, the interpretation depends on whether a single-particle gap $\Delta E_{\mathrm{TBA}} = 0$ or $\Delta E_{\mathrm{TBA}} > 0$. In the former case, occurring only for $t_y/t_x = 0.618$ (green dotted line) we recognize the semi-metallic phase (SM). Otherwise, the ground state can be identified as the band insulator (BI).

Unlike for bulk graphene, for which U_c monotonically decreases with $(t_x - t_y)/t_x$ [26], for $N_x = 10$ we observe an anomaly near $t_y/t_x = 0.618$ corresponding to $\Delta E_{\mathrm{TBA}} = 0$. The reduction of U_c can be attributed to the appearance of a nonzero density of states at the Fermi level, that could produce magnetic instability for (in principle) any $U > 0$. However, the value of $U_c \approx 0$ (away from $t_y/t_x = 0$) is not supported with our results. A series of approximations applied leads to $0 < U_c^{(\mathrm{HF})} < U_c^{(\mathrm{GA})} < U_c^{(\mathrm{SGA})}$ for any $0 < t_y/t_x \leqslant 1$. In particular, for $t_y/t_x = 0.618$ we obtain $U_c^{(\mathrm{HF})} = 1.21\,t_x$, $U_c^{(\mathrm{GA})} = 1.39\,t_x$, and $U_c^{(\mathrm{SGA})} = 1.82\,t_x$, each showing a significant (approximately a 40

percent) reduction in comparison to the bulk case. Probably, the competition of different insulating ground states, combined with quantum fluctuations, leads to the instability resulting in the appearance of a conducting phase, in a similar manner as earlier discussed on the examples of one-dimensional correlated nanosystems [37–40].

We further notice that the Variational Monte Carlo (VMC) results for $N_x = N_y = 10$, reprinted from Ref. [26] (datapoints with errorbars), are very close to the SGA results, showing that the latter can be regarded as a computationally-inexpensive counterpart to the former.

Next, in Fig. 3(b) and (c), we have fixed the Hubbard interaction at $U = 1.6\,t_x$ [24], and displayed the charge-energy gap for a correlated state,

$$\begin{aligned}\Delta E_C &= E_G^{(N_e=N+1)} + E_G^{(N_e=N-1)} - 2E_G^{(N_e=N)} \\ &\approx 2q(m,d) \min_{n_x,k_y} \sqrt{E_{\mathbf{k}} + (Um/2)^2},\end{aligned} \tag{13}$$

with N_e denoting the number of electrons and $q(m,d)$ given by Eq. (4), as a function of $(t_x - t_y)/t_x$. Here, the parameters (m,d) are optimized only once, for half filling ($N_e = N$); HF corresponds to a fixed $d = d_{\max}$; the gap following from Tight-Binding Approximation (TBA) is given by the first equality in Eq. (12).

Although a simple case of $N_x = 10$, showing the only one (non-trivial) zero of ΔE_{TBA}, is considered, quasiperiodic behavior of ΔE_C with increasing strain is already visible in Fig. 3(b). A zoom-in of the area surrounding $\Delta E_{\mathrm{TBA}} = 0$, presented in Fig. 3(c), shows that the multiparticle gap (ΔE_C) is reduced, comparing to the equilibrium value of $\Delta E_C \approx 0.35\,t_x$ for $t_y = t_x$, by a factor varying (depending on the method) from ~ 10 (HF) to ~ 100 (GA) when $t_y/t_x \approx 0.618$. (Notice that $U_c^{(\mathrm{SGA})} > 1.6\,t_x$ for such a range, and the semimetallic phase is predicted within SGA.) ΔE_C also shows two cusp-shaped maxima, located near $t_y/t_x = 0.309$ and 0.897, for which nearest values of k_x are equally distant from the Dirac point. In such cases, the role of electron correlations is negligible due to closed subbands (notice that the lines corresponding to different approximations overlap).

Significantly, a narrow gap following from GA for $t_y/t_x \approx 0.618$ ensures that ΔE_C becomes negligible in the presence of thermal excitations characterized by the energy of, say $\Delta E \approx t_0/100 \approx 25\,\mathrm{meV}$ (at $T = 300\,\mathrm{K}$), or a comparable energy of $e|V|$ due to source–drain voltage difference in transport experiment. In turn, for $U \approx 1.6\,t_x$ and $t_y/t_x \approx 0.618$, the semimetallic (or almost-semimetallic) behavior is predicted.

4. Conclusions

We have investigated, using the Gutzwiller approximation and related methods, the mutual effect of strain and electron–electron interaction on the ground state of semiconducting nanotube with zigzag edges. The results suggest that approximately 15% strain along the main axis may drive $(10,0)$ nanotube into the semimetallic phase. For weak Hubbard repulsion, we expect the semimetallic phase to reappear generically, for strains and winding numbers adjusted such that a single-particle gap vanishes. Most remarkably, quasiperiodic bandgap oscillations with the increasing strain are predicted. The analogy to the Aharonov-Bohm effect at nanoscale is put forward.

CRediT authorship contribution statement

Adam Rycerz: Conceptualization, Methodology, Software, Investigation and analysis, Writing. **Maciej Fidrysiak:** Methodology, Software, Investigation and analysis. **Danuta Goc-Jagło:** Project administration.

Declaration of competing interest

The authors declare that they have no known competing financial interests or personal relationships that could have appeared to influence the work reported in this paper.

Data availability

Data will be made available on request.

Acknowledgments

We thank Józef Spałek for discussions. Support from the National Science Centre of Poland (NCN), via Grant No. 2014/14/E/ST3/00256, at the early stage is acknowledged. Computations were partly performed using the PL-Grid infrastructure. All authors have read and agreed to the published version of the manuscript.

References

[1] D.Yu. Sharvin, Yu.V. Sharvin, Pis'ma Zh. Teor. Eksp. Fiz. 34 (1981) 285; JETP Lett. 34 (1981) 272.
[2] Y. Gefen, Y. Imry, M. Azbel, Phys. Rev. Lett. 52 (1984) 129.
[3] R.A. Webb, S. Washburn, C.P. Umbach, R.B. Laibowitz, Phys. Rev. Lett. 54 (1985) 2696.
[4] Yu.V. Nazarov, Ya.M. Blanter, Quantum Transport: Introduction To Nanoscience, Cambridge University Press, Cambridge, UK, 2009, http://dx.doi.org/10.1017/CBO9780511626906, Chapter 1.
[5] K.S. Novoselov, A.K. Geim, S.V. Morozov, D. Jiang, M.I. Katsnelson, I.V. Grigorieva, S.V. Dubonos, A.A. Firsov, Nature 438 (2005) 197.
[6] Y. Zhang, Y.-W. Tan, H.L. Stormer, P. Kim, Nature 438 (2005) 201.
[7] S. Russo, J.B. Oostinga, D. Wehenkel, H.B. Heersche, S.S. Sobhani, L.M.K. Vandersypen, A.F. Morpurgo, Phys. Rev. B 77 (2008) 085413.
[8] C. Stampfer, E. Schurtenberger, F. Molitor, J. Guettinger, T. Ihn, K. Ensslin, Internat. J. Modern Phys. 23 (2009) 2647.
[9] P. Recher, B. Trauzettel, A. Rycerz, Ya.M. Blanter, C.W.J. Beenakker, A.F. Morpurgo, Phys. Rev. B 76 (2007) 235404.
[10] A. Rycerz, Acta Phys. Polon. A 115 (2009) 322.
[11] M.I. Katsnelson, Europhys. Lett. 89 (2010) 17001.
[12] E.B. Kolomeisky, H. Zaidi, J.P. Straley, Phys. Rev. B 85 (2012) 073404.
[13] J. Schelter, P. Recher, B. Trauzettel, Solid State Commun. 152 (2012) 1411.
[14] A. Rycerz, D. Suszalski, Phys. Rev. B 101 (2020) 245429.
[15] F. de Juan, A. Cortijo, M.A.H. Vozmediano, A. Cano, Nat. Phys. 7 (2011) 810.
[16] S. Prabhakar, R. Nepal, R. Melnik, A.A. Kovalev, Phys. Rev. B 99 (2019) 094111.
[17] H. Ajiki, T. Ando, Phys. B 201 (1994) 349.
[18] U.C. Coskun, T.-C. Wei, S. Vishveshwara, P.M. Goldbart, A. Bezryadin, Science 304 (2004) 1132.
[19] D. Sangalli, A. Marini, Nano Lett. 11 (2011) 4052.
[20] F.-L. Shyu, Physica E 129 (2021) 114666.
[21] More detailed modelling suggests that the ground state of single wall nanotube zigzag edges may evolve from moderate- to narrow-gap semiconductor, the metallic phase is possible for armchair nanotubes; see Ref. [20].
[22] V.M. Pereira, A.H. Castro Neto, N.M.R. Peres, Phys. Rev. B 80 (2009) 045401.
[23] S. Sorella, Y. Otsuka, S. Yunoki, Sci. Rep. 2 (2012) 992.
[24] M. Schüler, M. Rösner, T.O. Wehling, A.I. Lichtenstein, M.I. Katsnelson, Phys. Rev. Lett. 111 (2013) 036601.
[25] L. Zhang, C. Ma, T. Ma, Phys. Status Solidi RRL 15 (2021) 2100287.
[26] G. Rut, M. Fidrysiak, D. Goc-Jagło, A. Rycerz, Int. J. Mol. Sci. 24 (2023) 1509.
[27] A.C. McRae, G. Wei, A.R. Champagne, Phys. Rev. Appl. 11 (2019) 054019.
[28] Y. Zheng, D. Sen, S. Das, S. Das, Piezoelectric Substr. : Nano Lett. 23 (2023) 2536.
[29] J. Jędrak, J. Kaczmarczyk, J. Spałek, e-print: arXiv:1008.0021 (unpublished).
[30] G.-W. Chern, K. Barros, C.D. Batista, J.D. Kress, G. Kotliar, Phys. Rev. Lett. 118 (2017) 226401.
[31] S.S. Gandhi, P.K. Patra, J. Phys.: Condens. Matter 33 (2021) 025001.
[32] Formally, approximation given in Eq. (8) also applies for the strain in a zigzag direction, $\varepsilon_y < 0$, $\varepsilon_x = -\nu\varepsilon_y > 0$.
[33] G. Dresselhaus, M.S. Dresselhaus, R. Saito, Physical Properties of Carbon Nanotubes, World Scientific, Singapore, 1998, http://dx.doi.org/10.1142/p080, Chapter 11.
[34] A. Rycerz, Phys. Rev. B 87 (2013) 195431.
[35] J.-C. Charlier, X. Blase, S. Roche, Rev. Modern Phys. 79 (2007) 677.
[36] E.H. Lieb, F.Y. Wu, Physica A 321 (2003) 1.
[37] Y. Gannot, Y.-F. Jiang, S.A. Kivelson, Phys. Rev. B 102 (2020) 115136.
[38] A. Rycerz, J. Spałek, Phys. Rev. B 63 (2001) 073101.
[39] J. Spałek, A. Rycerz, Phys. Rev. B 64 (2001) 161105(R).
[40] A.P. Kądzielawa, A. Biborski, J. Spałek, Phys. Rev. B 92 (2015) 161101(R).